

Effects of Dissolved Hydrogen on General Corrosion of Alloy 690TT and Boron Accumulation within its Oxide Films in PWR Primary Water

Soon-Hyeok Jeon, Geun Dong Song, Do Haeng Hur*

Nuclear Materials Safety Research Division, KAERI, 989-111 Daedeok-daero, Yuseong-gu, Daejeon 4057, Republic of Korea

*Corresponding author: dhhur@kaeri.re.kr

1. Introduction

In the primary water system of pressurized water reactors (PWRs), general corrosion leads to Ni release from the surface of steam generator (SG) tubes. Co is also released to reactor coolants from the SG tube materials containing impurity Co (0.014 wt.% max). Released Ni-58 and Co-59 are activated to Co-58 and Co-60 in the reactor core by a neutron flux, respectively [1] and act as the primary source of high radiation fields in the primary system [2].

Furthermore, these corrosion products are deposited on the surface of fuel cladding. The deposited corrosion products are called crud (Chalk River Unidentified Deposits). The crud deposition on fuel cladding can have the negative effects on the fuel performance and fuel cladding integrity. In addition, boron can be hide-out in the pores of thick crud in the boiling region of fuel cladding. As boron accumulates within the crud deposits, neutrons are absorbed locally causing measurable power shifts from the top of the core to the lower half of the core, called axial offset anomaly (AOA) or crud induced power shift (CIPS) [3,4]. Therefore, it is apparent that the corrosion products mitigation released from the SG tubes should be an important strategy for source term reduction in PWRs.

The corrosion behavior of SG tube will be affected by water chemistry. Among the water chemistry parameters, many investigations related to dissolved hydrogen (DH) concentration have focused on the crud deposition of fuel cladding and PWSCC of SG tube in primary water of PWRs [5,6]. However, the effect of DH concentration on the general corrosion and boron accumulation within the oxide films of Alloy 690TT in primary water of PWRs has not been reported.

In this study, with an increase in DH content from 5 to 100 cm³/kg H₂O, the structure of oxide films, general corrosion behavior, and associated boron accumulation within the oxide films formed on Alloy 690TT was studied in simulated primary water at 330 °C. Based on a relationship between the general corrosion rate and PWSCC susceptibility by various DH concentrations, operation condition of DH concentration in primary water of PWRs is also discussed.

2. Methods

2.1 Material preparation

Alloy 690TT tubes, which are commonly used as a steam generator tubing material, were used in this study. The chemical composition of Alloy 690TT is given in Table 1. The specimen has a dimension of 19.07-mm outer diameter (OD) and a 16.93-mm inner diameter (ID) with a 50-mm length. The specimens for corrosion test have a hole of 3 mm in diameter to hang on a specimen tree in the autoclave. Some specimens were also cut into 10 mm x 10 mm x 1.07 mm for a surface oxide analysis.

Table 1. Chemical composition of Alloy 690TT (wt.%).

C	Al	Si	Ti	Cr	Mn	Fe	Ni
0.02	0.1	0.1	0.1	28.0	0.3	10.2	Bal.

2.2 Corrosion tests

Corrosion tests were performed in an autoclave connected to a primary water recirculating system, which was shown schematically in Fig. 1. Test solution under a hydrogen overpressure was injected from the feed tank through a high-pressure pump to the test vessel with a flow rate of 20 ml/min. The corrosion test was performed at 330 °C under 150 bars in the autoclave for 500 h without shutdown. Simulated primary water was prepared using high purity demineralized water and nuclear-grade lithium hydroxide (LiOH) and boric acid (H₃BO₃). The test solution was 2.2 ppm Li, and 1,200 ppm B in weight.

The DH concentration was controlled to 5, 10, 35, 50, 65, 100 cm³/kg H₂O at standard temperature and pressure (STP) by controlling the hydrogen overpressure of the solution tank. Dissolved oxygen (DO) was controlled to be less than 5 ppb to eliminate the effects of oxygen on the specimen surface.

Chemical descale methodology was applied to obtain the general corrosion rate of Alloy 690TT. The corrosion products of oxidized specimen were removed by multiple applications of the two-step alkaline permanganate (AP) and ammonium citrate (AC) descaling process. The oxidation step was done in a 1% potassium permanganate (KMnO₄) and 5% sodium hydroxide (NaOH) solution; the dissolution step was done in a 5% diammonium citrate solution. Each step was conducted by immersion in a water bath for 3 min at 90 °C. After two steps, the weight loss of the specimens was measured using a 5-place balance with an accuracy of ±0.04 mg.

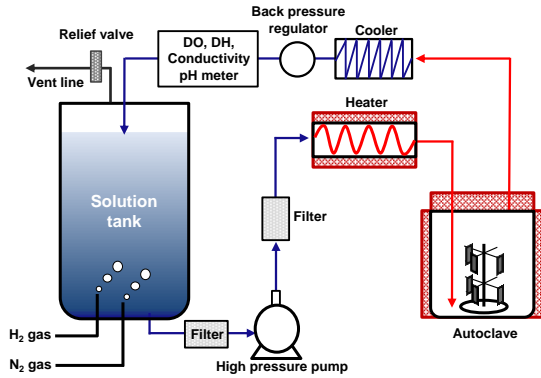


Fig. 1. Schematic of the corrosion test loop system.

2.3 Analysis of oxide films

The morphology of oxide films formed on Alloy 690TT specimens was observed using scanning electron microscope (SEM). The focus ion beam (FIB) milling technique was used to prepare the transmission electron microscope (TEM) samples, allowing us to produce samples of which the oxide film structure could be observed in depth. The line analyses of oxide films were performed using an energy dispersive X-ray spectroscopy (EDS) attached to the TEM. To elucidate the oxide film structure and associated boron accumulation within the oxide layer, the depth profile and chemical species of the oxide layers were analyzed using X-ray photoelectron spectrometer (XPS). XPS with an Al K α X-ray source (1486.6 eV) operated at 15 kV and 150 W under a base pressure of 2.7×10^{-7} Pa. The binding energies of all peaks were corrected by the reference C1s peak at 284.5 eV.

2.4 Calculation of corrosion potentials

Ni-based alloys and stainless steels behave as a hydrogen electrode in hydrogenated water at high temperatures in previous investigations [7-9]. Hence, if we know the DH concentration, temperature, Henry's law coefficient and pH_T , the corrosion potentials (E_{corr}) of Alloy 690 can be calculated versus the standard hydrogen scale (SHE) by using the Nernst equation for the hydrogen-hydrogen ion exchange reaction ($2H^+ + 2e^- = H_2$). Equation (1) is the simplified Nernst equation:

$$E_{SHE} = -4.308 \times 10^{-5} \cdot T \{ \ln(H \cdot [H_2]) + 4.606 pH_T \} \quad (1)$$

In this test conditions, the necessary data to calculate the E_{corr} of Alloy 690TT are summarized as follows: $T = 603$ K, $H = 7.88 \times 10^{-3}$ atm/(cm³ STP/kg H₂O) and $pH_T = 7.4010$. $[H_2]$ is the dissolved hydrogen concentration.

3. Results and discussion

Fig. 2 shows the SEM morphologies of the oxide films formed on Alloy 690TT in the DH range of 5-100

cm³/kg H₂O. The surface morphologies of oxide films were significantly changed with DH concentration. As shown in Fig. 2 (a), the oxide film was covered with numerous filament-like oxides and several large planar oxide particles at DH = 5 cm³/kg H₂O. Many filament-like oxides were randomly tangled with a filament diameter of less than 100 nm. The many planar oxide particles were dispersed on the filament-like oxides. The size of planar oxide particles were with a size of 150-400 nm. Under the conditions of DH = 10 cm³/kg H₂O, a great number of filament-like oxides were observed without the planar oxide particles (Fig. 2 (b)). The diameter of filament-like oxides at DH = 10 cm³/kg H₂O were much larger than that of filament-like oxides at DH = 5 cm³/kg H₂O. As shown in Fig. 2 (c)-(f), in the DH range of 35-100 cm³/kg H₂O, the morphology of the oxide films significantly changed. The fine polyhedral oxide particles were formed on the surface of specimens. These oxide particles were with a size of 20-200 nm. The number of the oxide particles decreased with increasing the DH concentration.

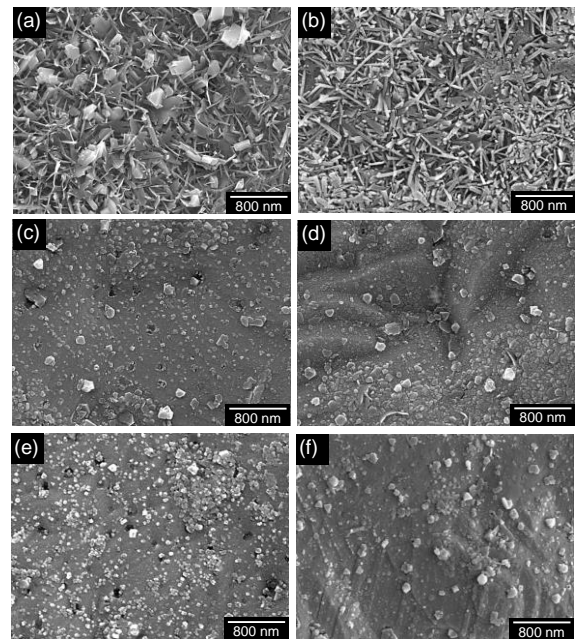


Fig. 2. SEM images of the oxide films formed on Alloy 690TT in primary water with various DH concentrations at 330 °C: (a) 5 cm³/kg H₂O, (b) 10 cm³/kg H₂O, (c) 35 cm³/kg H₂O, (d) 50 cm³/kg H₂O, (e) 65 cm³/kg H₂O, and (f) 100 cm³/kg H₂O.

Fig. 3 shows the TEM images and line scan analysis of the cross section of oxide films formed on Alloy 690TT. At DH = 5 cm³/kg H₂O, a double-layered structure was formed: an outermost layer with Ni oxide and inner layer with Cr₂O₃. The inner Cr₂O₃ layer was both homogeneous and continuous. Under the conditions of DH = 35 cm³/kg H₂O, a triple-layered structure was formed: outer polyhedral spinel oxides such as NiCrFeO₄, a middle metallic Ni-rich layer, and Cr₂O₃ layer located in the inner part. The inner Cr₂O₃

layer formed at $DH = 35 \text{ cm}^3/\text{kg}$ appeared not to be continuous in this case.

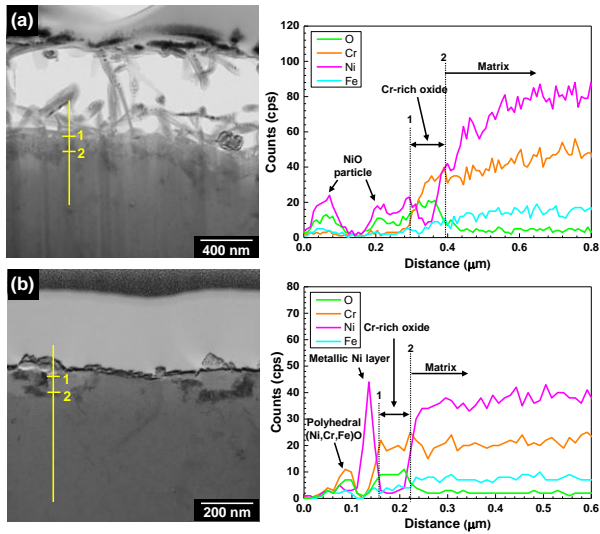


Fig. 3. TEM images and line EDS analyses of cross section of oxide films formed on Alloy 690TT in simulated primary water with various DH concentrations at $330 \text{ }^\circ\text{C}$: (a) $5 \text{ cm}^3/\text{kg}$ H_2O and (b) $35 \text{ cm}^3/\text{kg}$ H_2O .

Fig. 4 presents the depth profile of chemical species on the oxide films formed on Alloy 690TT with sputtering time in primary water with $DH = 5$ and $50 \text{ cm}^3/\text{kg}$ H_2O at $330 \text{ }^\circ\text{C}$. The outer part of oxide layer formed at $DH = 5 \text{ cm}^3/\text{kg}$ H_2O consisted predominantly of Ni^{2+} , as shown in Fig. 4 (a). By contrast, Cr^{3+} and Ni^0 were primarily located in the inner part of oxide layer under this condition. These results indicate that the double-structured oxide layers consisted of Ni oxide layer with inner Cr_2O_3 layer were formed at $DH = 5 \text{ cm}^3/\text{kg}$ H_2O , which is in good agreement with the present findings shown in Fig. 3. In the oxide layer formed at $DH = 50 \text{ cm}^3/\text{kg}$ H_2O , the outer part of oxide layer was predominantly composed of Ni^{2+} . The Ni^{2+} and Cr^{3+} concentration gradually decreased and Ni^0 concentration increased with increase of sputtering time. Finally, the Ni^0 dominated in the inner part of oxide layer. These results were attributed to the triple-structured oxide layer formed at $DH = 50 \text{ cm}^3/\text{kg}$ H_2O : outer polyhedral spinel oxides such as NiCrFeO_4 , a middle metallic Ni-rich layer, and Cr_2O_3 layer located in the inner part. However, in this case, the inner Cr_2O_3 layer was not detected because the inner Cr_2O_3 layer may be formed to be discontinuous. The B^{3+} was observed at the outer oxide surface at $DH = 5 \text{ cm}^3/\text{kg}$ H_2O . The concentration of B^{3+} was weakened with increase of sputtering time. However, the B^{3+} was not observed at $DH = 50 \text{ cm}^3/\text{kg}$ H_2O . These results indicate that the boron compounds could be accumulated in the porous oxide layer at $DH = 5 \text{ cm}^3/\text{kg}$ H_2O , whereas the hideout of boron compounds did not occur in the dense polyhedral oxide layer at $DH = 50 \text{ cm}^3/\text{kg}$ H_2O .

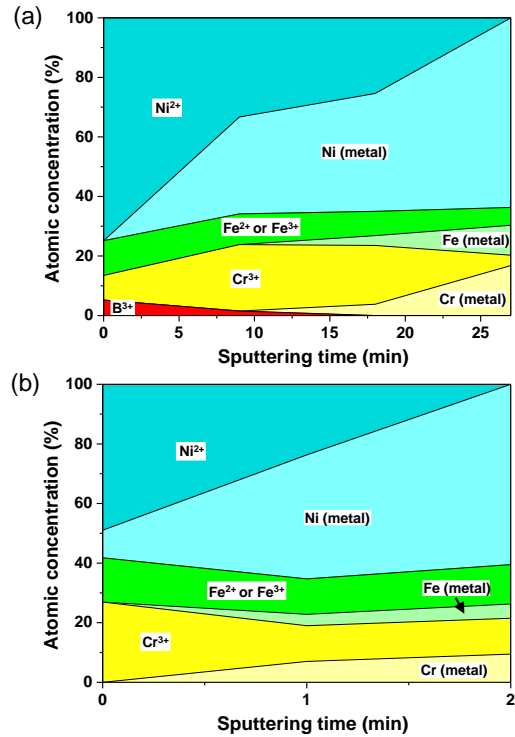


Fig. 4. The depth profile of chemical species on the oxide films formed on Alloy 690TT with sputtering time in primary water with $DH = 5$ and $50 \text{ cm}^3/\text{kg}$ H_2O at $330 \text{ }^\circ\text{C}$: (a) $5 \text{ cm}^3/\text{kg}$ H_2O and (b) $50 \text{ cm}^3/\text{kg}$ H_2O .

Fig. 5 shows the E_{corr} values of Alloy 690TT with various DH concentrations. The E_{corr} of Alloy 690TT decreased with increasing DH concentration. In addition, the DH concentration at the Ni/NiO transition line was calculated using the following equation (2) obtained from Andresen et al.: [10]

$$\log C_H = 0.0111 \times (T - 273) - 2.59 \quad (2)$$

where C_H is the DH concentration in high-temperature water (cm^3/kg H_2O) at the Ni/NiO phase transition line and T is the temperature of the water (K). At $330 \text{ }^\circ\text{C}$, the calculated Ni/NiO phase boundary corresponded to the DH concentration of $11.8 \text{ cm}^3/\text{kg}$ H_2O .

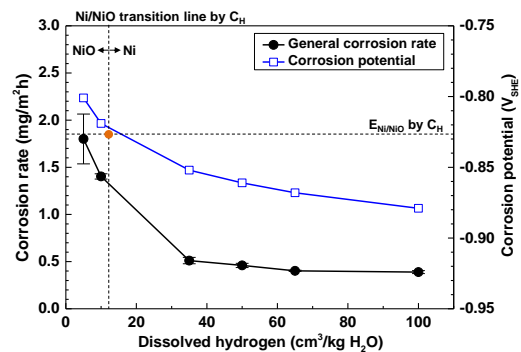


Fig. 5. General corrosion rates and corrosion potentials of Alloy 690TT with various DH concentrations.

In EPRI Guidelines, the content of DH has been specified to be controlled in a range of 25-50 cm³/kg H₂O [1]. Hydrogen related researches have mainly been focused on the stress corrosion cracking of structural materials in the primary water (PWSCC). Many investigations have reported that the crack growth rate (CGR) of Ni-based alloys at a given temperature varies with DH concentration (Fig. 6). The CGR shows a maximum peak at a DH concentration approximately corresponding to the Ni/NiO phase transition line [11,12], and decreases as DH concentrations deviate from the peak point. However, as shown in Fig. 6, the effect of hydrogen on crack initiation time seems a little inconsistent or relatively small [13,14]. Alloy 600 has been replaced with Alloy 690TT and no corrosion damage of Alloy 690TT including SCC has been reported since its application to PWRs. Therefore, we think that the focus regarding DH concentration should be changed from PWSCC to general corrosion. This is because the released corrosion products through general corrosion are the sources of radiation field and AOA. From Fig. 5, the general corrosion rate decreases as the DH concentration increases. This means that the control of DH in the upper part of the 25 to 50 cm³/kg H₂O range or beyond the upper limit of 50 cm³/kg H₂O is positive effect for not only mitigation of PWSCC but also general corrosion.

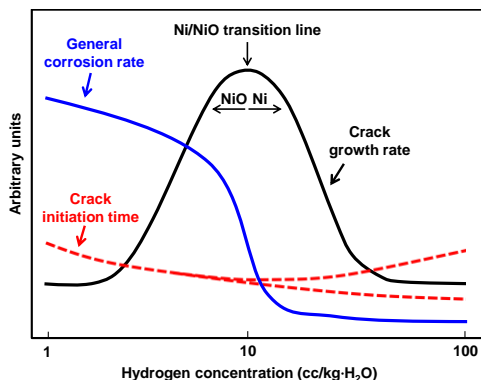


Fig. 6. Schematic of effect of DH contents on the general corrosion rate and PWSCC susceptibility (crack growth rate and crack initiation time) of Ni-based alloys in primary water of PWRs.

4. Conclusions

(1) In simulated primary water of PWRs at 330 °C, the double-structured oxide layers consisted of thick porous Ni oxide layer with inner Cr₂O₃ layer were formed at low DH range (5-10 cm³/kg H₂O). Under the medium and high DH range (35-100 cm³/kg H₂O), the dense triple-structured oxide layers grew thinner and consisted of an outer polyhedral spinel oxide particles and an intermediate metallic Ni-rich layer, with inner Cr₂O₃ layer.

(2) Boron compounds could be accumulated in the porous Ni oxide layer, whereas the hideout of boron

compounds did not occur in the dense polyhedral oxide layer.

(3) The general corrosion rate significantly decreased by approximately 72% as DH content increased from 5 to 35 cm³/kg H₂O. In the DH range of 35-65 cm³/kg H₂O, the corrosion rate slightly decreased with increasing DH content. However, the corrosion rate slightly decreased in the range of 65-100 cm³/kg H₂O. Our group thinks that these results are worthwhile for mitigation the general corrosion behavior of Alloy 690TT tubing in the primary water of PWRs.

ACKNOWLEDGEMENTS

This work was supported by the National Research Foundation of Korea (NRF) grant funded by the Korea government (MSIP) (2017M2A8A4015159).

REFERENCES

- [1] EPRI-1014986, Pressurized Water Reactor Primary Water Chemistry Guidelines, Vol. 1, Revision 6, EPIR, Palo Alto, CA, USA, 2007.
- [2] EPRI-NP-6737, Cobalt Reduction Guidelines, EPRI, Palo Alto, CA, USA, 1990.
- [3] W. Byers, J. Deshon, Structure and chemistry of PWR crud, in: Proceeding of the International Conference on Water Chemistry of Nuclear Reactor Systems, San Francisco, USA, October 11-14, 2004.
- [4] J. Henshaw, J. McGuire, H. Sims, A. Tuson, S. Dickinson, The Chemistry of Fuel Deposits and Its Effect on AOA in PWR Plants, in: Proceeding of the International Conference on Water Chemistry of Nuclear Reactor System, Jeju, Korea, October 23-26, 2006.
- [5] Q. Peng, J. Hou, K. Sakaguchi, Y. Takeda, T. Shoji, Electrochim. Acta. 56 (2011) 8375-8386.
- [6] J. Xu, T. Shoji, C.H. Jang, Corros. Sci. 97 (2015) 115-125.
- [7] M.E. Indig and C. Groot, Corrosion 26 (1970) 171-176.
- [8] W.K. Lai and Z. Szklarska-Smialowska, Corrosion 47 (1991) 40-47.
- [9] S.A. Attanasio, D.S. Morton and M.A. Ando, CORROSION 2002, Paper 02517, NACE (2002)
- [10] P.L. Andresen, J. Hickling, A. Ahluwalia, J. Wilson, Corrosion 64 (2008) 707-720.
- [11] D. S. Morton, S. A. Attanasio, J. S. Fish, M. K. Schurman, Influence of Dissolved Hydrogen on Nickel Alloy SCC in High-Temperature Water, Paper 447, Corrosion'99, Texas, USA, April 25-30, NACE: Houston, TX, 1999.
- [12] D. S. Morton, S. A. Attanasio, G. A. Young, Primary Water SCC Understanding and Characterization Through Fundamental Testing in the Vicinity of the Nickel/Nickel Oxide Phase Transition, Proceedings of the Tenth International Symposium on Environmental Degradation of Materials in Nuclear Power Systems-Water Reactors, Lake Tahoe, Nevada, USA, August 5-9, NACE: Houston, TX, 2001
- [13] EPRI-1012145, Materials Reliability Program: Effects of Hydrogen, pH, Lithium, and Boron on Primary Water Stress Corrosion Crack Initiation in Alloy 600 for Temperatures in the Range 320-330 °C (MRP-147) EPRI, Palo Alto, CA, USA, 2005.
- [14] N. Totsuka, E. Lunarska, G. Cragolino, Z. Szklarska-Smialowska, Corrosion 43 (1987) 505-514.